Inflammation (2023) 46:1796–1809
https://doi.org/10.1007/s10753-023-01842-1

RESEARCH

Protective Effect of a Novel RIPK1 Inhibitor, Compound 4–155, in Systemic Inflammatory Response Syndrome and Sepsis

Zhong-Yi Ling[1,2] , Quan-Zhen Lv[2] , Jiao Li[2] , Ren-Yi Lu[2] , Lin-Lin Chen[2] , Wei-Heng Xu[2] , Yan Wang[1,2,3] and Chun-Lin Zhuang[2,3]

Received 17 February 2023; accepted 16 May 2023

Abstract— Excessive inflammatory response is a critical pathogenic factor for the tissue damage and organ failure caused by systemic inflammatory response syndrome (SIRS) and sepsis. In recent years, drugs targeting RIPK1 have proved to be an effective anti-inflammatory strategy. In this study, we identified a novel anti-inflammatory lead compound 4–155 that selectively targets RIPK1. Compound 4–155 significantly inhibited necroptosis of cells, and its activity is about 10 times higher than the widely studied Nec-1 s. The anti-necroptosis effect of 4–155 was mainly dependent on the inhibition of phosphorylation of RIPK1, RIPK3, and MLKL. In addition, we demonstrated that 4–155 specifically binds RIPK1 by drug affinity responsive target stability (DARTS), immunoprecipitation, kinase assay, and immunofluorescence microscopy. More importantly, compound 4–155 could inhibit excessive inflammation *in vivo* by blocking RIPK1-mediated necroptosis and not influence the activation of MAPK and NF-κB, which is more potential for the subsequent drug development. Compound 4–155 effectively protected mice from TNF-induced SIRS and sepsis. Using different doses, we found that 6 mg/kg oral administration of compound 4–155 could increase the survival rate of SIRS mice from 0 to 90%, and the anti-inflammatory effect of 4–155 *in vivo* was significantly stronger than Nec-1 s at the same dose. Consistently, 4–155 significantly reduced serum levels of pro-inflammatory cytokines (TNF-α and IL-6) and protected the liver and kidney from excessive inflammatory damages. Taken together, our results suggested that compound 4–155 could inhibit excessive inflammation *in vivo* by blocking RIPK1-mediated necroptosis, providing a new lead compound for the treatment of SIRS and sepsis.

KEY WORDS: compound 4–155; RIPK1; necroptosis; systemic inflammatory response syndrome; sepsis.

Zhong-Yi Ling and Quan-Zhen Lv contributed equally to this work.

[1]School of Pharmacy, Fujian University of Traditional Chinese Medicine, Fuzhou, China
[2]School of Pharmacy, Second Military Medical University, Shanghai 200433, China
[3]To whom correspondence should be addressed at and School of Pharmacy, Fujian University of Traditional Chinese Medicine, Fuzhou, China. Email: wangyansmmu@126.comSchool of Pharmacy, Second Military Medical University, Shanghai, 200433, China. Email: zclnathan@163.com

INTRODUCTION

Systemic inflammatory response syndrome (SIRS) is an exaggerated inflammatory response caused by infection, tumor, surgery, ischemia reperfusion, and other infectious or non-infectious factors [1]. The release of acute-phase inflammatory mediators and cytokines, such as TNF-α, IL-1, IL-6, and IL-8, causes endothelial cell damage, platelet adhesion, and the production of oxygen free radicals. The inflammatory mediators could further promote the activation of inflammatory cells and expand the inflammatory response persistently. The dysregulated inflammatory responses will result in reversible and irreversible organ damage [2]. Although sepsis is re-defined as a more complex disease than the inflammatory response in 2016 [3], SIRS is still closely related to the high mortality of sepsis. Sepsis is a main cause of in-hospital deaths, which accounted for about 10% of deaths in intensive care units (ICU) [4]. Globally, patients suffering from sepsis worldwide were about 48.9 million per year, of which 11 million patients died, accounting for approximately 20% of deaths all around the world [5–7]. At present, available drugs to treat SIRS and sepsis are limited and could not effectively solve the problem of immune dysregulation [8].

Lipopolysaccharide (LPS) is a major cause of exaggerated inflammatory responses and quick sequential organ failure during sepsis [9]. Immune cells stimulated by LPS secrete a large number of pro-inflammatory cytokines, such as TNF-α, IL-1, and IL-6. LPS and the high levels of TNF-α could result in cell necroptosis, a caspase-independent programmed death [10]. Unlike apoptosis and autophagy, necroptosis leads to cell membrane rupture and the leakage of intracellular substances, which further exacerbates the inflammatory response [11]. Therefore, blocking necroptosis is an effective means to reduce the excessive inflammatory response in SIRS and sepsis. As reported, TNF-α combined with caspase-8 inhibitor Z-VAD-fmk could induce necroptosis through activating the phosphorylation of receptor-interacting protein kinases 1 and 3 (RIPK1/3). Then, phosphorylated RIPK3 recruits mixed lineage kinase domain-like protein (MLKL) and actives it by phosphorylation. The phosphorylated MLKL changes conformation and forms a tetramer, which could remove to the membrane and induce cell death [12–14]. RIPK1 has been extensively studied. It is not only involved in the necroptosis, but also in MAPK/NF-κB-dependent regulation of cell proliferation and survival. The binding of TNF-α and TNFR1 could recruit proteins with the death domain to form complex I, which leads to the ubiquitination of RIPK1. Ubiquitinated RIPK1 form a complex with Ikappa B kinase (IKK) and TGF β-activated kinase (TAK) to activate the nuclear factor-kappa B (NF-κB). Moreover, the TNF-stimulated NF-κB and mitogen-activated protein kinases (MAPK) signaling could be further enhanced by the interaction of linear ubiquitinated RIPK1 and other TNFR1-recruited proteins [15]. Activation of MAPK and NF-κB signaling is critical for cell survival, cell differentiation, inflammatory responses, and apoptosis [16]. Abnormal MAPK and NF-κB activity is known to be closely associated with inflammatory diseases, autoimmune diseases, metabolic diseases, and cancer [17]. In general, selective blocking of RIPK1-mediated necroptosis without affecting the activation of MAPK and NF-κB signaling pathways is more promising for new drug development.

RIPK1 inhibitors have been extensively studied for the treatment of a variety of diseases, such as SIRS, sepsis, neurodegenerative diseases, and ischemic injury [18]. According to the different binding sites of compounds, RIPK1 inhibitors are mainly divided into 4 classes, including type I ATP enzyme inhibitors, type II ATP enzyme inhibitors, type III kinase inhibitors, and others [19]. Among them, Necrostatin-1 s (Nec-1 s) was reported as the first small-molecule inhibitor of RIPK1 and used extensively as a tool in many animal models and mechanistic studies, as its metabolic stability *in vivo* was enhanced compared with Necrostatin-1 [20]. Meanwhile, Nec-1 s showed no influence on the activation of MAPK and NF-κB signaling pathways and selectively blocked RIPK1-mediated necroptosis, which got more promising at new drug development [21, 22].

In this study, we synthesized a new compound 4–155, which exhibited a significantly stronger anti-necroptosis effect than Nec-1 s. Compound 4–155 targets RIPK1, selectively inhibits the phosphorylation of RIPK1, RIPK3, and MLKL, and has no effect on the activation of MAPK and NF-κB. The compound showed strong efficacy in both SIRS and cecal ligation puncture (CLP) induced sepsis in mice, indicating that our study will provide a new direction for drug development against excessive inflammatory responses.

MATERIALS AND METHODS

Biological Reagents

Compound 4–155 was synthesized by our lab as reported previously. Compound 4–155 was purified

to > 95% determined by high-performance liquid chromatography (HPLC) analysis and fully identified by 1H-NMR, 13C-NMR, and HRMS [23]. Recombinant mouse mTNF-α (CF09) was obtained from Novoprotein. Recombinant human TNF-α (GMP-TL303) was obtained from T&L Biological Technology. Human TNF-α was used in the stimulation of human colorectal adenocarcinoma cells (HT-29) and mouse fibroblasts cells (L929) *in vitro*, and mTNF-α (CF09) was used in the mouse model of SIRS. PMSF was obtained from Beyotime. Anti-human antibodies: RIP1 (3493) and phospho-RIP1 (65746 s), phospho-MLKL (91689 s), and GAPDH (D16H11) were obtained from Cell Signaling Technology. Anti-RIP3 (phospho S227) (ab209384) and MLKL (ab184718) were obtained from Abcam. NF-κB p65 (D14E12), phospho-NF-κB p65 (Ser536), IκBα (L35A5), phospho-IκBα (Ser32), MAPK/JNK Antibody (9252), phospho-MAPK/JNK (Thr183/Tyr185), p44/42 MAPK (ERK1/2) (137F5), and phospho-p44/42 MAPK (ERK1/2) (Thr202/Tyr204) (D13.14.4E) were purchased from Cell Signaling Technology. HRP-conjugated Affinipure Goat Anti-Mouse IgG (H + L) (SA00001-1) and HRP-conjugated Affinipure Goat Anti-Rabbit IgG (H + L) (SA00001-2) were obtained from Proteintech. Anti-mouse antibodies: Anti Phospho-RIP1(38662) and RIP1 (3493) antibodies were obtained from Cell Signaling Technology, and RIP3 (17563–1-AP) was obtained from Proteintech. Anti-RIP3 (phospho T231 + S232) (ab222320) was obtained from Abcam. Antibodies for immunofluorescence: Anti-RIP1(3493) and Anti-RIP3(10188), Anti-rabbit IgG (H + L), F(ab')2 Fragment (Alexa Fluor 594 Conjugate) (8889) and Anti-Rabbit IgG (H + L), F(ab')2 Fragment (Alexa Fluor 488 Conjugate) (4412) were obtained from Cell Signaling Technology.

Cell Culture

HT-29 (NCI-DTP Cat# HT-29, RRID: CVCL_0320) and L929 (ECACC Cat# 14112101, RRID: CVCL_AR58) cells were cultured in DMEM mediums containing 1% streptomycin/penicillin and 10% FBS in a humidified atmosphere of 5% CO_2 at 37 °C as reported previously [24].

Anti-Necroptosis Activity Assays

The necroptosis was induced as described with a few modifications [25]. Necroptosis of HT-29 cells was caused by pretreatment with Smac mimetic (10 nmol/L) and Z-VAD-fmk (20 mol/L) for 0.5 h followed by incubation with TNF-α (20 ng/mL) for the mentioned time. Compound 4–155 or Nec-1 s were added simultaneously with Smac mimetic and Z-VAD-fmk. The necroptosis of L929 cells was induced by Z-VAD-fmk and TNF-α without Smac mimetic. The cell viability was measured by the Cell Counting Kit-8 (Beyotime, C0037). All experiments were performed at least three times independently.

Immunoblotting

The immunoblotting was assayed as described previously [26]. After compound 4–155 and Nec-1 s intervention, the cells were lysed by cell lysis buffer for western blot and immunoprecipitation (IP) (Beyotime Biotechnology, P0013) containing protease/phosphatase inhibitors (Beyotime Biotechnology, P1046) and PMSF (Beyotime Biotechnology ST506). The protein samples (40 ng) were resolved over 10% SDS-PAGE and transferred to nitrocellulose (NC) membranes. According to the molecular weight of proteins, the NC membrane was horizontally divided into two parts, which was coated with antibodies to GAPDH and target protein, respectively. The membranes were then blocked in 5% non-fat powdered milk (Beyotime Biotech, P0216), incubated with primary antibodies (1:1000) and secondary antibody (1:10000) that diluted in 5% milk. The blotting results were analyzed by the Tanon-5200Multi system. After scanning, the target protein strip was cleaned with the Western stripping buffer (Beyotime Biotechnology, P0025B) for 5 min, and the solution was discarded. Then, the NC membrane was washed with PBST for 3 times and incubated with the new target protein antibody. The new band was scanned by the Tanon-5200Muti system and repeat the stripped and reprobed operation until all the target proteins were successfully scanned. The western blot strip grayscale was processed by the Image J software.

Kinase Assay

The inhibitory effects on RIP1 and RIP3 kinases were detected by a KINOMEscan™ assay as described previously [24]. Briefly, the RIPK1 kinase lysate was tagged with DNA for qPCR detection. The binding reaction of 4–155, RIPK1 kinase, and liganded affinity beads was conducted in 1 × binding buffer (6 mM Dithiothreitol, 20% SeaBlock, 0.05% Tween 20, and 0.17 × PBS). Equilibrium K_D was determined from the concentration of 5 μM. Different concertation of 4–155 was obtained by triple dilution with DMSO. The qPCR detection was

performed in a polypropylene 384-well plate. The assay plates were incubated at room temperature for 1 h. Then, the affinity beads were washed with PBS containing 0.05% Tween 20. The liganded affinity beads were then resuspended in elution buffer (1 × PBS, 0.05% Tween 20, and 0.5-μM non-biotinylated affinity ligand) and incubated at room temperature for 30 min. The kinase elution was measured by qPCR.

Immunoprecipitation

After treatment with compound 4–155 or Nec-1 s for 6 h, HT-29 cells were lysed and incubated with anti-RIP1 antibody and Protein A/G agarose successively at 4 °C for 2 days. The immunoprecipitated proteins were obtained by boiling in 5 × SDS buffer and examined by western blot analysis.

Determination of Drug Affinity Responsive Target Stability (DARTS)

The determination of stability of drug affinity reactivity targets was conducted as described previously [24]. The cell lysis was incubated with compound 4–155 at room temperature for 1 h and then digested with 0.1% of pronase for 30 min. The digestion was stopped by directly adding SDS-PAGE loading buffer and boiling. Protein samples were separated with 10% SDS-PAGE and analyzed by immunoblotting.

Immunofluorescence Microscopy

HT-29 cells were treated with Smac mimetic (10 nmol/L), Z-VAD-fmk (20 mol/L), and 4–155 (1 μM) for 0.5 h followed by incubation with TNF-α (20 ng/mL) for 6 h. Then, cells were washed with PBS for 3 times and fixed with 500 μl 4% neutral polyformaldehyde for 15 min. After fixation, 250 μl 0.5% Triton X-100 was added. Cells were incubated at room temperature for 20 min and washed with PBS for 3 times. Subsequently, cells were incubated overnight with RIPK3 antibody at 4 ℃ and then washed with PBST. Next, samples were incubated with Alexa Fluo 488-conjugated rabbit secondary antibody for 1 h and washed with PBST for 3 times. Then, cells were incubated with RIPK1 antibody for about 12 h at 4 ℃ and washed with PBST for 3 times. Alexa Fluo 594-labeled secondary antibody was added at room temperature and stained for 1 h and then washed with PBST for 3 times. Finally, cells were counterstained with 10 μg/ml 4′,6-diamidino-2-phenylindole (DAPI) for 5 min. Images were obtained by Leica DMi fluorescence microscope.

Hematoxylin and Eosin (H&E) Staining

Lung and kidney tissues were obtained from the control group and three groups of SIRS mice treated with PBS, 6 mg/kg Nec-1s, or 4-155 for 24 h, respectively. Among 5 mice in each group, 3 mice were randomly selected. The tissues of the 3 mice were fixed with 4% paraformaldehyde and embedded with paraffin. Each paraffin block was sliced at 4 μm and stained with hematoxylin and eosin (Beyotime C0105M).

TNF-Induced SIRS Model

Animal experiments are approved by the Animal Care Committee of the Second Military Medical University (Shanghai, China) and conducted as described previously [27]. Male C57/BL6 mice (weight 18–22 g) were obtained from Regan Biology and given compound 4–155 or Nec-1 s orally 1 h before intravenous injection of mTNF-α (350 μg/kg). A total of 200 μg of Z-VAD-fmk was injected intraperitoneally in 15 min before mTNF-α injection. Another dose of Z-VAD-fmk was injected 1 h after mTNF injection. The anal temperature of mice was measured by the intelligent digital thermometer (Thermometer model, TH212, Sichuan Zhongsheng Hong Technology Co., Ltd).

Cecal Ligation and Puncture Model

The cecal ligation and puncture model was conducted as described previously [26, 28]. Mice were given 6 mg/kg of compound 4–155 or Nec-1 s orally 1 h before anesthesia by injection of pentobarbital sodium. Remove hair from the midline of the abdomen to expose the skin, cut an opening of 1–1.5 cm under sterile conditions, and take out the cecum. Ligate about 50% of the cecum with 4–0 medical silk braid, puncture both sides with 22 G needles, gently squeeze the ligated cecum, squeeze a little content from the two puncture holes, and carefully return the cecum. Suture the incision layer by layer with medical silk braid, and povidone-iodine was used for postoperative disinfection. After these steps, the mouse was immediately resuscitated by normal saline at 37 °C (1 ml per 20 g body weight) subcutaneously. Besides, appropriate measures were taken to alleviate the pain of mice. The mice in the sham operation group (Sham) were treated with CLP mice except for cecal ligation and puncture.

ELISA Assay

The serum of SIRS and CLP mice was collected at 6 h and 24 h, respectively, after modeling. The ELISA kits used in this study include Mouse IL-6 ELISA Kit (mlbio, ml063159), Mouse TNF-α ELISA Kit (mlbio, ml002095), Alanine aminotransferase Assay Kit (Nanjing Jiangcheng Bioengineering Institute, C009-2–1), Aspartate aminotransferase Assay Kit (Nanjing Jiancheng Bioengineering Institute, C013-2–1), Urea Assay Kit (Nanjing Jiancheng Bioengineering Institute, C013-2–1), and Creatinine (cr) Assay kit (sarcosine oxidase) (Nanjing Jiancheng Bioengineering Institute, C011-2–1). All tests were carried out in accordance with the manufacturer's instructions.

The Statistical Analysis

Our results are presented as means ± SD. Gray ratios of protein detected by Western Blot were analyzed by Image J software. The normality of the distribution was assessed by the Kolmogorov–Smirnov tests. One-way ANOVA followed by Tukey or Dunnett's post-hoc tests and log-rank (Mantel-Cox) test were performed for data analysis using GraphPad Prism 8.0 software.

RESULTS

Compound 4–155 Inhibits Necroptosis *In Vitro* by Inhibiting RIPK1-RIPK3-MLKL Pathway

Necroptosis could be triggered by TNF-α or FasL under the blockage of caspase by zVAD-fmk [29]. In this study, the necroptosis of HT-29 and L929 cells was induced by TNF-α, Smac mimetic, and Z-VAD-fmk (TSZ). Cell survival was assayed by CCK-8. The structure of compound 4–155 is shown in Fig. 1A. Our results showed that 4–155 exhibited a dose-dependent inhibitory effect on TSZ-induced necroptosis. On both HT-29 and L929 cells, 0.031 μM of 4–155 exhibited a protective effect on about 80% of cells, while Nec-1 s showed similar protective effects at a concentration up to 0.5 μM (Fig. 1B and C). These results indicated that 4–155 is a more effective necrosis inhibitor than Nec-1 s.

To investigate whether compound 4–155 and Nec-1 s protect cells from necroptosis by inhibiting RIPK1-RIPK3-MLKL pathway, we detected the phosphorylation of RIPK1, RIPK3, and MLKL by western blot. Both 4–155 and Nec-1 s could completely inhibit the phosphorylation of RIPK1, RIPK3, and MLKL in HT-29 cells at 1 μM after treatment time as short as 2 h (Fig. 2A). Further studies revealed dose-dependent effects of both 4–155 and Nec-1 s, with 4–155 showing better potency. More specifically, both 4–155 and Nec-1 s inhibited the phosphorylation of RIPK1, RIPK3, and MLKL in a dose-dependent manner in a range of 0.01 to 1 μM. They both inhibited the phosphorylation of RIPK1, RIPK3, and MLKL at the highest concentration of 1 μM in this study. Regarding 4–155, it completely inhibited the phosphorylation of RIPK1, RIPK3, and MLKL at 0.1 μM. While for Nec-1 s, to inhibit the phosphorylation of RIPK1, RIPK3, and MLKL, the concentration should reach 1 μM (Fig. 2B). We further investigated the minimum effective concentration of 4–155, and the results indicated that at the concentration as low as 0.02 μM, 4–155 significantly inhibited the phosphorylation of RIPK1, RIPK3, and MLKL (Fig. 2C). Collectively, these results indicated that 4–155 blocked necroptosis by inhibiting the activation

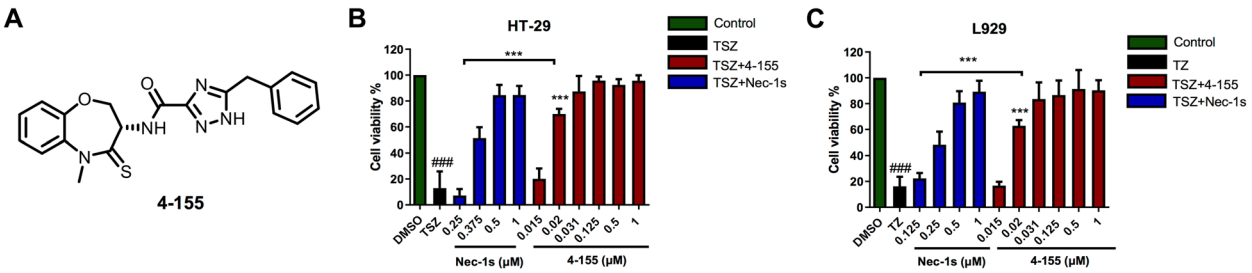

Fig. 1 Compound 4–155 protects HT-29 and L929 cells from necroptosis. **A** The structure of compound 4–155. **B**, **C** Necroptosis of HT-29 and L929 cells. HT-29 cells (**B**) and L929 cells (**C**) were treated with 4–155 or Nec-1 s at the specified concentrations and then stimulated with TSZ or TZ, respectively, for 24 h. Data shown are the mean ± SD and tested by one-way ANOVA followed by Tukey's post-hoc test, $^{###}P < 0.001$ (model verification), $^{**}P < 0.01$, $^{***}P < 0.001$.

of RIPK1-RIPK3-MLKL pathway, and its activity is significantly higher than Nec-1 s.

Compound 4–155 Inhibits Necrosis by Selectively Targeting RIPK1 and Shows No Effect on the Activation of MAPK and NF-κB Pathways

The direct binding of Nec-1 s to RIPK1 has been clearly demonstrated previously [30–32]. In this study, drug affinity responsive target stability (DARTS) was carried out to confirm the direct interactions between 4–155 and RIPK1. DARTS relies on the reduced protease sensitivity of drug-binding proteins. When the total proteins were incubated with protease, the drug-binding proteins were resistant to proteolysis [33]. As expected, 4–155 significantly improved the stability of RIPK1 to protease digestion. In contrast, the stability of RIPK3 and MLKL was not improved by 4–155 (Fig. 3A). To further investigate the affinity between compound 4–155 and RIPK1, we detected the blocking effect of compound 4–155 on the combination of specific DNA-tagged RIPK1 and liganded affinity beads. Our results showed that compound 4–155 inhibited the ligand binding of RPIK1 dose-dependently, and the equilibrium Kd was determined as 31 nM (Fig. 3B). These results indicated that 4–155 may selectively bind with RIPK1 to protect cells from necroptosis. Necroptosis was medicated by the interaction between RIPK1 and RIPK3 through their RIP homotypic interaction motifs [34]. The binding of RIPK1 and RIPK3 could form a structure of "necrosome," resulting in the phosphorylation of downstream MLKL [35]. It has been reported that Nec-1 s could block the interaction between RIPK1 and RIPK3 [36]. Thereby, we speculated that 4–155 may also affect the binding of

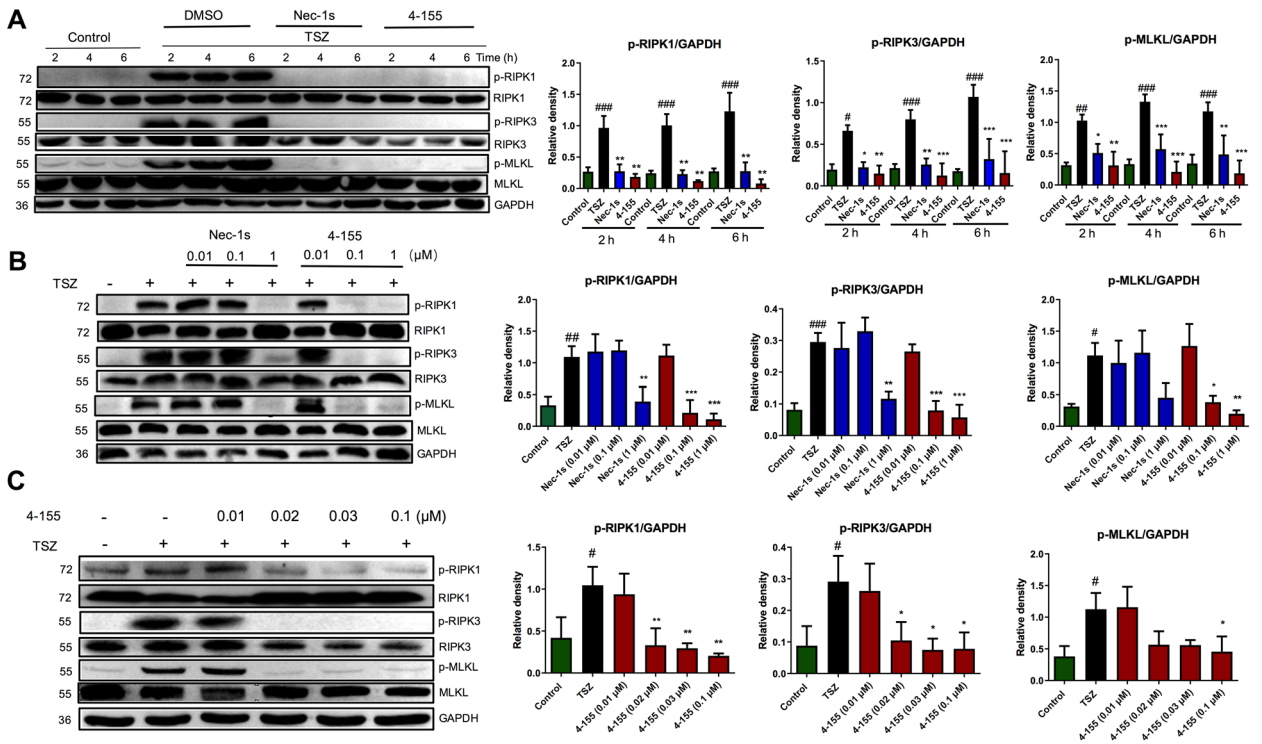

Fig. 2 Compound 4–155 inhibits the phosphorylation of RIPK1, RPK3, and MLKL. Immunoblot analysis and quantification of p-RIPK1, p-RIPK3, and p-MLKL were carried out. **A** HT-29 cells were pretreated with 1 μM 4–155 or Nec-1 s and stimulated with TNF-α for 15 min, 30 min, and 60 min, respectively. **B** HT-29 cells were pretreated with 0.01 μM, 0.1 μM, or 1 μM of 4–155 or Nec-1 s and stimulated with TSZ for 6 h. **C** HT-29 cells were pretreated with 4–155 (0.01, 0.02, 0.03, and 0.1 μM) and stimulated with TSZ for 6 h. The gray ratios between phosphorylated protein and GAPDH were analyzed by the Image J software and shown in the right panel. Data shown are the mean ± SD and tested by one-way ANOVA followed by Dunnett's post-hoc test, and the effects of Nec-1 s and 4–155 were significant compared with TSZ-treated cells. $^{\#}P<0.05$ (model verification), $^{\#\#}P<0.01$ (model verification), $^{\#\#\#}P<0.001$ (model verification), $^{*}P<0.05$, $^{**}P<0.01$, $^{***}P<0.001$.

RIPK1 and RIPK3. By using immunoprecipitation, we found that the addition of 4–155 or Nec-1 s resulted in the failure of RIPK1 antibody to pull down RIPK3, indicating that both 4–155 and Nec-1 s could significantly inhibit the binding between RIPK3 and RIPK1 (Fig. 3C). Yuan *et al*. revealed that RIPK and RIPK3 could form mosaic necrosomes [37]. To investigate the effect of 4–155 on the interaction between RIPK1 and RIPK3, we observed the formation of necrosomes in HT-29 cells using immunofluorescence microscopy. Our results showed that TSZ stimulation could significantly induce the colocalization of RIPK1 and RIPK3 significantly. However, 4–155 treatment resulted in RIPK3 being dispersed in cells and not co-localized with RIPK1 (Fig. 3D). This result confirmed that 4–155 disrupted the binding of RIPK1 and RIPK3, suggesting that 4–155 can directly target RIPK1 and regulate the necroptosis of cells.

As reported, the kinase function of RIPK1 not only mediates the necroptosis, but also plays a platform role for the activation of MAPK and NF-κB [38]. In order to determine whether JNK, ERK, and NF-κB activation could be affected by 4–155, we examined cells exposed to TNF-α stimulation. Our results showed that phosphorylation of JNK, ERK, p65, and IκBα was significantly activated in HT-29 cells after 15 min, 30 min, and 60 min treatment with TNF-α. However, the activation of p-JNK, p-ERK, p-p65, and p-IκBα was not affected by the addition of 1 μM 4–155 or Nec-1 s (Fig. 4A and B). These

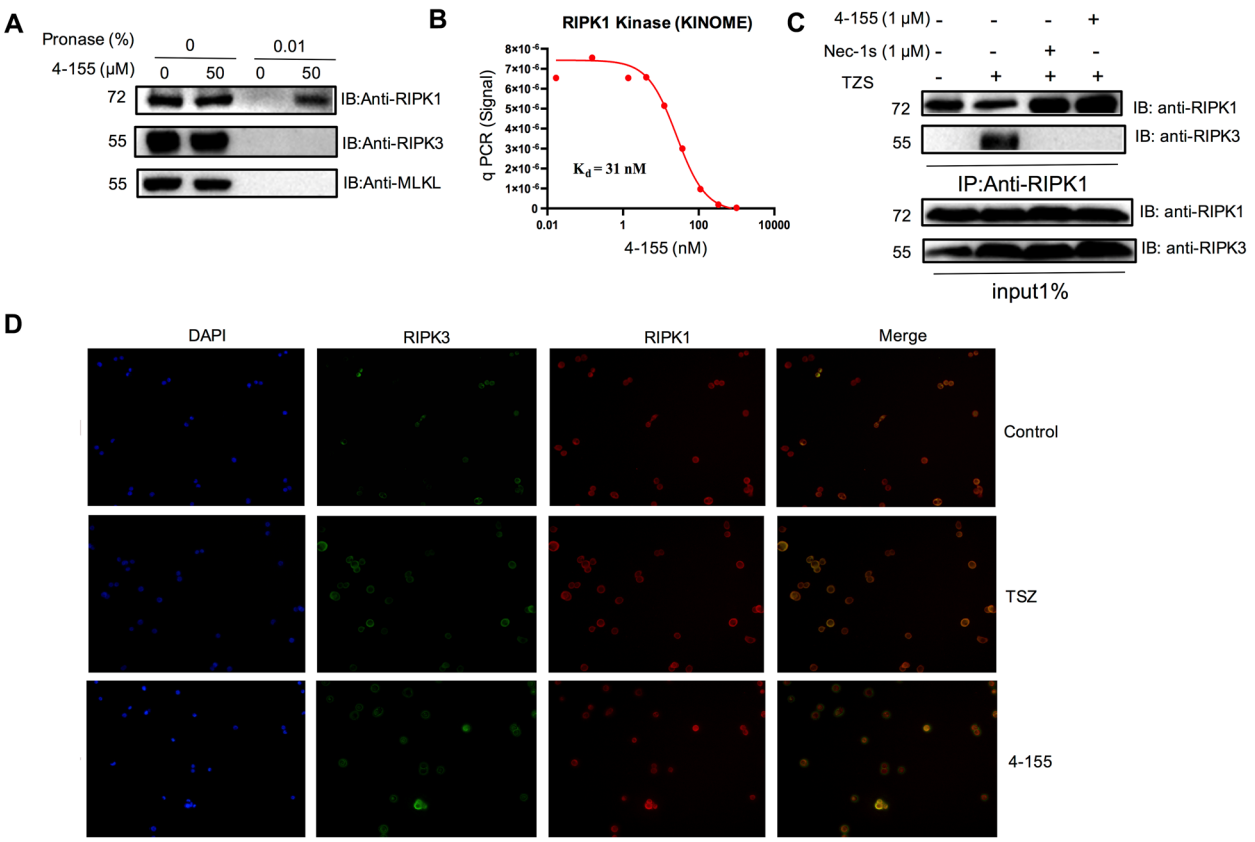

Fig. 3 Compound 4–155 binds to RIPK1 specifically. **A** DARTS analysis of RIPK1, RIPK3, and MLKL treated with 4–155. The total proteins of HT-29 cells were incubated with 50 μM 4–155 and digested with 0.1% of pronase for 30 min at room temperature. **B** K_D values of 4–155 against recombinant RIPK1 kinase were measured by KINOMEscan™ assay. Compound 4–155, RIPK1 kinase tagged with DNA, and liganded affinity beads were incubated at room temperature for 1 h. **C** The interaction of RIPK1 and RIPK3 was detected by immunoprecipitation. HT-29 cells were treated with 1 μM of 4–155 or Nec-1 s for 6 h. Cell lysate was immunoprecipitated with anti-RIPK1 antibody. **D** Immunofluorescence of RIPK1 and RIPK3 in HT-29 cells. HT-29 cells were stimulated with TSZ and treated with 1 μM 4–155 for 6 h.

results indicate that 4–155 can selectively block the interaction between RIPK1 and RIPK3, but does not affect the activation of MAPK and NF-κB pathways.

Compound 4–155 Is More Effective than Nec-1 s in mTNF-Induced SIRS

To explore the anti-inflammatory activity of 4–155 *in vivo*, we first investigated it in a murine SIRS model induced by mTNF-α. By observing the survival rate, we found that 4–155 had protective effects at 0.7 mg/kg, 2 mg/kg, 6 mg/kg, and 18 mg/kg doses, and the survival rate increased by 30%, 60%, 90%, and 100%, respectively. Meanwhile, 4–155 showed a better protective effect than Nec-1 s at all four doses (Fig. 5A and B). Consistently, 4–155 more effectively reversed SIRS-induced hypothermia (Fig. 5C–F). We further evaluated the protective effect of 4–155 on liver and kidney damages in the SIRS model. By biochemical analysis of serum, we found that the treatment of 4–155 decreased the levels of aspartate transferase (AST), alanine aminotransferase (ALT), creatinine, and blood urea nitrogen (BUN) significantly at 6 mg/kg. Of note, 4–155 treatment was significantly more effective than Nec-1 s in reducing AST, ALT, serum creatinine, and BUN, indicating the excellent effects of 4–155 (Fig. 5G–J). In addition, 4–155 treatment significantly reduced levels of the pro-inflammatory

Fig. 5 Compound 4–155 protects mice from TNF-induced SIRS. **A**, **B** ▶ Survival analysis of mice treated with 4–155 or Nec-1 s ($n=10$). **C**–**F** Body temperature of mice treated with compound 4–155 or Nec-1 s ($n=5$). **G**, **H** Liver function analysis of mice treated with 4–155 or Nec-1 s. Serum AST and ALT was measured by ELISA. **I**, **J** Kidney function analysis of mice treated with 4–155 or Nec-1 s. Serum creatinine and blood urea nitrogen (BUN) were measured by ELISA. **K**, **L** Pro-inflammatory cytokines TNF-α and IL-6 measured by ELISA. **M** Inflammatory infiltration of lung and kidney analyzed by hematoxylin–eosin staining. Blue arrows indicate the accumulation of inflammatory cells in the lungs and kidneys. Male C57/BL6 mice were given 0.7 kg/kg, 2 mg/kg, 6 mg/kg, and 18 mg/kg of 4–155 or Nec-1 s orally 1 h before intravenous injection of mTNF-α (350 μg/kg). In addition, 200 μg of Z-VAD-fmk was injected intraperitoneally in 15 min before mTNF-α injection. The survival curves were analyzed by log-rank test. Panels **C**–**L** are shown as the mean ± SD and tested by one-way ANOVA followed by Tukey's post-hoc test. $^{\#\#}P<0.01$ (model verification), $^{\#\#\#}P<0.001$ (model verification). $^{*}P<0.05$, $^{**}P<0.01$, $^{***}P<0.001$, ns, no significant, vs vehicle group. The significance marked on the lines represents the differences between the two groups connected by the lines.

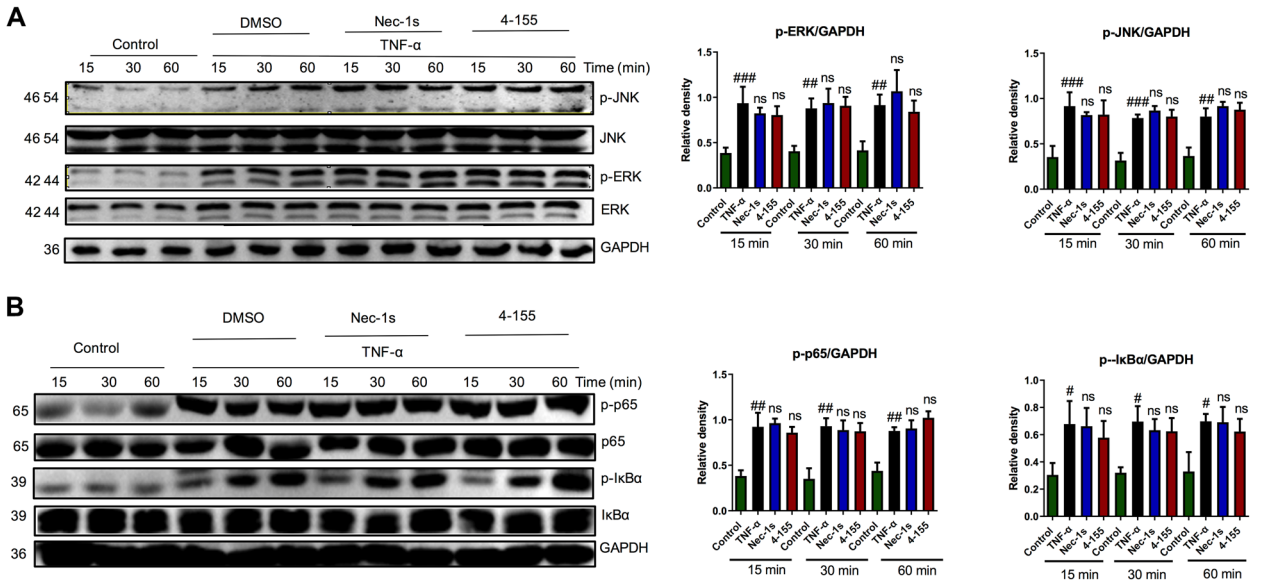

Fig. 4 The activation of MAPK and NF-κB was not affected by compound 4–155. **A** Immunoblot analysis and quantification of p-JNK and p-ERK. **B** Immunoblot analysis and quantification of p-p65 and p-IκBα. HT-29 cells were pretreated with 1 μM 4–155 or Nec-1 s for 30 min and then stimulated with 20 ng/ml TNF-α for 15 min, 30 min, and 60 min, respectively. The gray ratios between phosphorylated protein and GAPDH were analyzed by the Image J software and shown in the right panel. Data shown are the mean ± SD and tested by one-way ANOVA, followed by Dunnett's post-hoc test, and the effects of Nec-1 and 4–155 were significant compared with the TNFα-treated cells, $^{\#}P<0.05$ (model verification), $^{\#\#}P<0.01$ (model verification), $^{\#\#\#}P<0.001$ (model verification), ns, no significant.

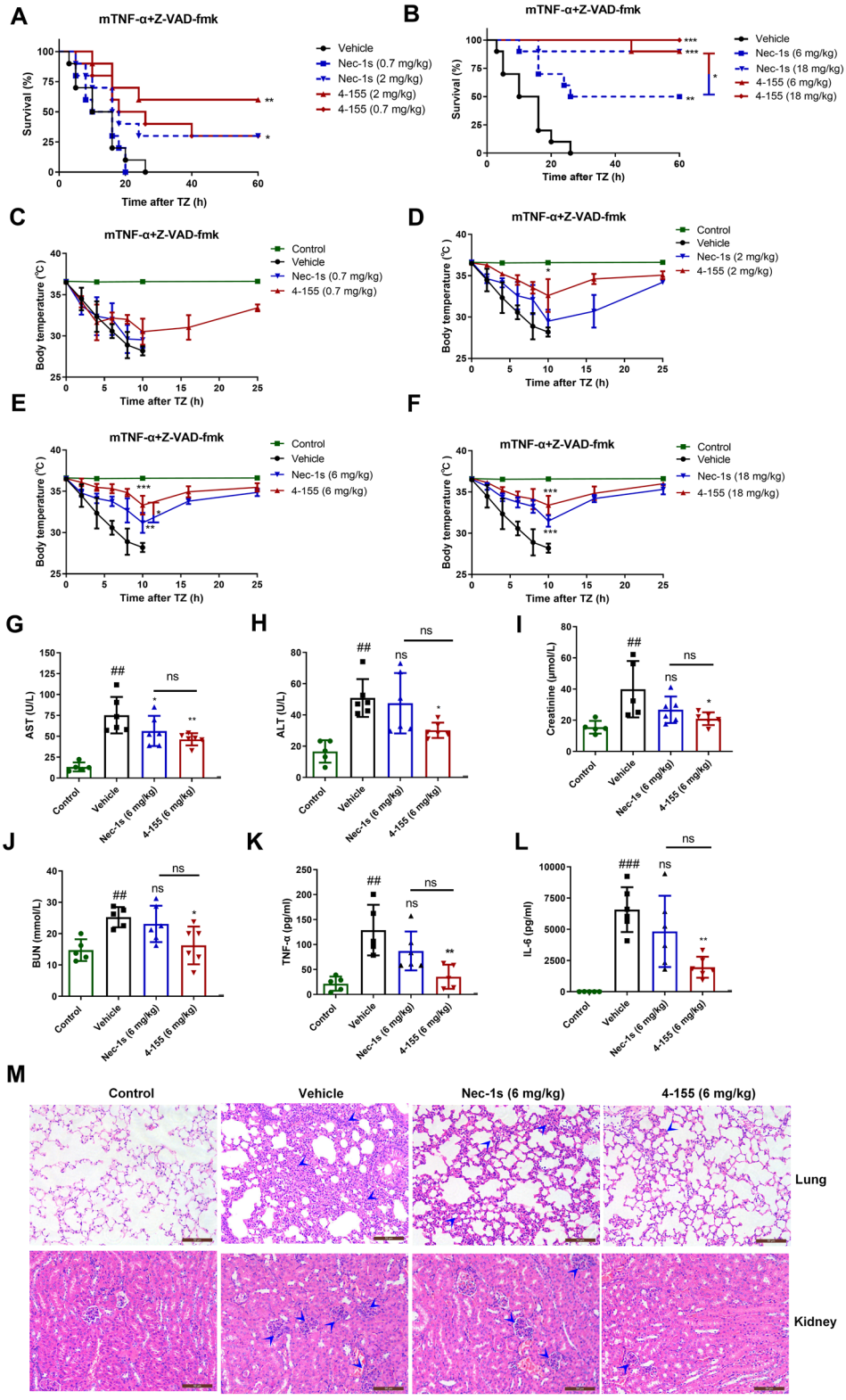
A
mTNF-α+Z-VAD-fmk
Survival (%)
Time after TZ (h)
Vehicle
Nec-1s (0.7 mg/kg)
Nec-1s (2 mg/kg)
4-155 (2 mg/kg)
4-155 (0.7 mg/kg)
B
mTNF-α+Z-VAD-fmk
Survival (%)
Time after TZ (h)
Vehicle
Nec-1s (6 mg/kg)
Nec-1s (18 mg/kg)
4-155 (6 mg/kg)
4-155 (18 mg/kg)
C
mTNF-α+Z-VAD-fmk
Body temperature (℃)
Time after TZ (h)
Control
Vehicle
Nec-1s (0.7 mg/kg)
4-155 (0.7 mg/kg)
D
mTNF-α+Z-VAD-fmk
Body temperature (℃)
Time after TZ (h)
Control
Vehicle
Nec-1s (2 mg/kg)
4-155 (2 mg/kg)
E
mTNF-α+Z-VAD-fmk
Body temperature (℃)
Time after TZ (h)
Control
Vehicle
Nec-1s (6 mg/kg)
4-155 (6 mg/kg)
F
mTNF-α+Z-VAD-fmk
Body temperature (℃)
Time after TZ (h)
Control
Vehicle
Nec-1s (18 mg/kg)
4-155 (18 mg/kg)
G
AST (U/L)
H
ALT (U/L)
I
Creatinine (μmol/L)
J
BUN (mmol/L)
K
TNF-α (pg/ml)
L
IL-6 (pg/ml)
Control
Vehicle
Nec-1s (6 mg/kg)
4-155 (6 mg/kg)
M
Control
Vehicle
Nec-1s (6 mg/kg)
4-155 (6 mg/kg)
Lung
Kidney

cytokines TNF-α and IL-6 compared with the vehicle group (Fig. 5K and L). Hematoxylin–eosin (HE) staining of the lungs and kidneys also showed that 4–155 treatment significantly reduced inflammatory cell infiltration (Fig. 5M). HE staining showed blue-purple nuclei and pink cytoplasm. For inflammatory cells, the volume ratio of the nucleus to the cytoplasm is high. In this study, we found significant thickening of alveolar walls in the SIRS group, consistent with an increase in blue-purple areas indicating increased inflammatory cell infiltration. Both Nec-1 s and 4–155 resulted in thinning of the alveolar walls in SIRS mice, and the thickness of the alveolar walls in 4–155 treated mice was more similar to that in control healthy mice. In addition, compound 4–155 protected normal alveolar morphology with thin alveolar septum, reduced infiltration of inflammatory cells, and no congestion or edema. Regarding kidneys in the vehicle group, more areas were stained blue-purple, indicating accumulation of inflammatory cells. In contrast, only slight accumulation of inflammatory cells was observed in the 4–155 treatment group, similar to the control group and less than the Nec-1 s treatment group.

In general, these results indicated that 4–155 had an effective protective effect on mTNF-induced SIRS in mice, and its activity *in vivo* is higher than that of Nec-1 s.

Compound 4–155 Protected Mice from Organ Damage and Excessive Inflammation Caused by CLP

To further evaluate the anti-inflammatory effect of 4–155, we tested its therapeutic effect on inflammation caused by severe infections. In a cecal ligation puncture model, we found that 6 mg/kg treatment of 4–155 improved survival by 30% compared to Nec-1 s treatment by 10% (Fig. 6A). To investigate the protective effects on liver and kidney functions, we tested serum AST, ALT, creatinine, and BUN contents. The contents of AST, ALT, creatinine, and BUN in the 6 mg/kg Nec-1 s group were not significantly different from those in the untreated group. In contrast, 6 mg/kg 4–155 significantly reduced serum AST, ALT, creatinine, and BUN levels in the CLP model (Fig. 6B–E). Consistently, treatment with 4–155 significantly reduced levels of the pro-inflammatory cytokines TNF-α and IL-6, but Nec-1 s did not reduce the levels of these factors (Fig. 6F and G). Our results further confirm that 4–155 had higher anti-inflammatory activity than Nec-1 s. As a syndrome caused by dysregulated host responses to infection, CLP-induced polymicrobial sepsis has been shown to be closely associated with pyroptosis [39]. To investigate the role of necroptosis in sepsis, we investigated the activation of p-RIPK1 and p-RIPK3 in renal cells of septic mice. Western blot results showed that the phosphorylation level of RIPK3 in the kidney of septic mice was significantly increased, and the levels of p-RIPK1 and p-RIPK3 were reduced in mice treated with 6 mg/kg of 4–155. Meanwhile, Nec-1 s slightly reduced the phosphorylation of RIPK1 and RIPK3, but the difference was not statistically significant. Consistent with the protective effects, 4–155 could decrease the phosphorylation of RIPK1 and RIPK3 more significantly than Nec-1 s (Fig. 6H and I). Collectively, our results suggest that 4–155 has a stronger inhibitory effect on RIPK1-dependent necroptosis than Nec-1 s, both *in vitro* and *in vivo*.

DISCUSSION

SIRS and sepsis are the main cause of in-hospital deaths, which could result in tissue damage and organ failure [40]. Nevertheless, drugs available for the treatment of SIRS and sepsis are very limited in the clinic. In this study, we discovered a new compound, 4–155, with a strong anti-inflammatory effect both *in vitro* and *in vivo* by specifically targeting RIPK1. The anti-necroptosis activity of 4–155 in HT-29 and L929 cells was approximately tenfold higher than that of the positive control drug Nec-1 s. The DARTS and co-immunoprecipitation results showed that 4–155 could specifically bind to RIPK1, which blocked the formation of Complex IIb and inhibited the phosphorylation of RIPK1, RIPK3, and MLKL. In SIRS and sepsis models, the protective effect of 4–155 was stronger than that of Nec-1 s in mice. Overall, our results suggest that 4–155 has potential for clinical application.

The targeting of RIPK1 by compound 4–155 was confirmed by DARTS, RIPK1 kinase assay, and co-immunoprecipitation. By detecting the stability changes of RIPK1, RIPK3, and MLKL under the pronase digestion, we found that only the stability of RIPK1 increased after the treatment of 4–155. The co-immunoprecipitation clearly demonstrated that 4–155 blocked the binding of RIPK1 and RPIK3. As 4–155 did not change the stability of RIPK3 to pronase digestion, we believe that 4–155 could interact with RIPK1 directly. As the target of 4–155, RIPK1 has been studied widely for its role in inflammatory diseases, such as SIRS [41], sepsis [42], virus infection [43], and autoinflammatory diseases including rheumatoid

and ulcerative colitis [44, 45]. In recent years, inhibitors targeting RIPK1 have become a hot topic in drug development [46, 47]. Nec-1 s was the first inhibitor of RIPK1 and was used extensively as a positive control or tool compound in preclinical studies [20]. Through widely screening, the selectivity of Nec-1 s was confirmed as > 1000 fold for RIPK1 than any other 485 human kinases [48]. Although *in vivo* stability of Nec-1 s was enhanced through the modification of Nec-1, its oral administration activity still needs to be further improved [36].

In this study, we identified a new oral compound 4–155 that is more active than Nec-1 s both *in vitro* and *in vivo*. In addition, compound 4–155 avoids the MAPK and NF-κB inhibition problems of RIPK1 inhibitors. By detecting the phosphorylation of JNK, ERK, p65, and IκBα, the effect of 4–155 on the activation of MAPK and

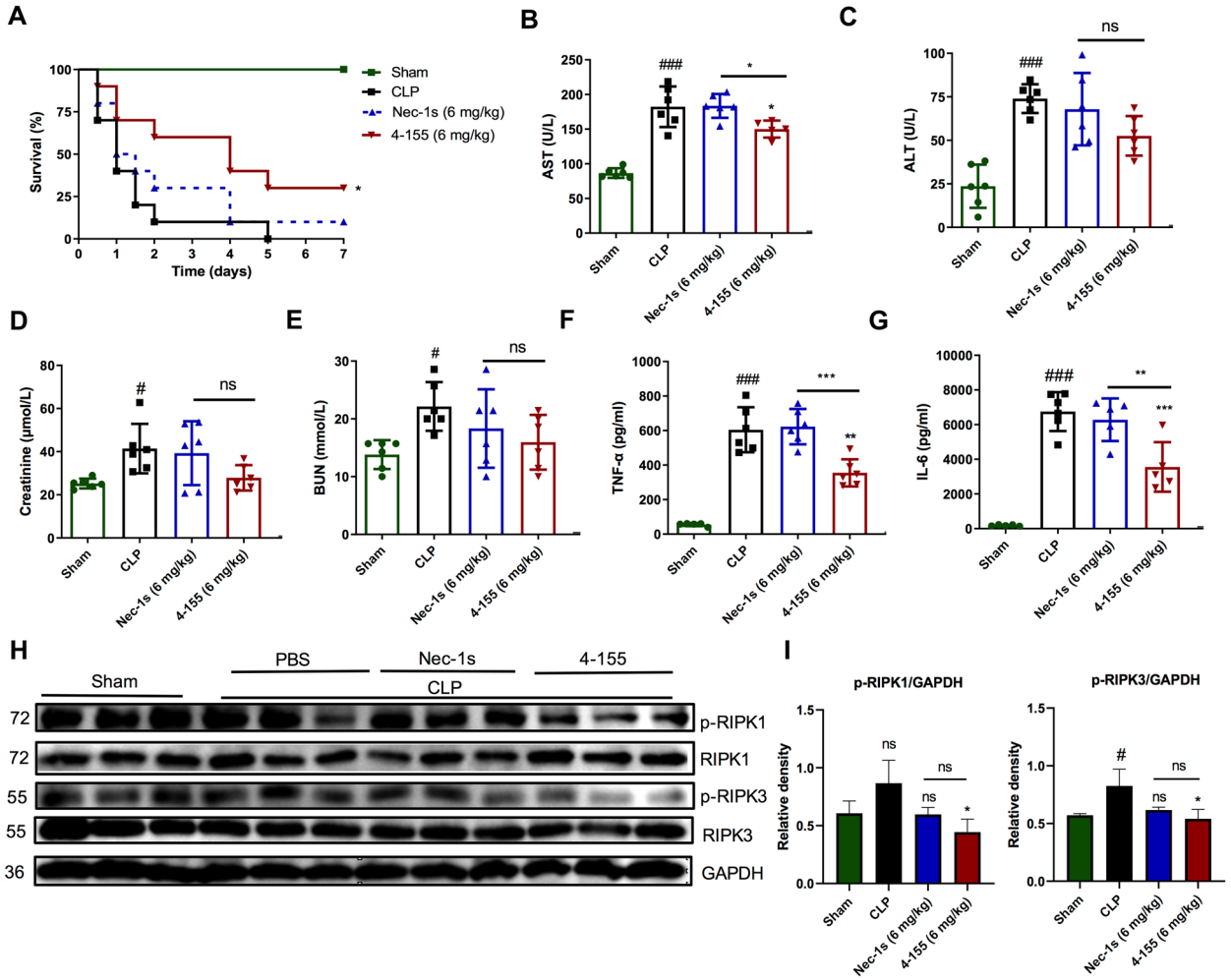

Fig. 6 Compound 4–155 protects mice from sepsis cause by CLP. **A** Survival analysis of septic mice treated with 4–155 or Nec-1 s ($n = 10$). **B**, **C** Liver function analysis of mice treated with 4–155 or Nec-1 s. Serum AST and ALT was measured by ELISA ($n = 6$). **D**, **E** Kidney function analysis of mice treated with 4–155 or Nec-1 s. Serum creatinine and blood urea nitrogen (BUN) were measured by ELISA ($n = 6$). **F**, **G** Pro-inflammatory cytokines TNF-α and IL-6 measured by ELISA ($n = 6$). **H** Immunoblot analysis of p-RIPK1 and p-RIPK3 in whole kidney lysates ($n = 3$). **I** The gray ratios between phosphorylated protein and GAPDH quantified by Image J software. Male C57/BL6 mice were pretreated with 6 mg/kg of 4–155 or Nec-1 s for 1 h and then induced sepsis by cecal ligation puncture. Serum and the whole kidney lysates were collected after cecal ligation and puncture for 6 h. The survival curves were analyzed by log-rank test. Panels **B**–**G** and **I** are shown as the mean ± SD and tested by one-way ANOVA followed by Tukey's post-hoc test. $^{###}P < 0.001$ (model verification). $^{*}P < 0.05$, $^{**}P < 0.01$, $^{***}P < 0.001$, ns, no significant, vs vehicle group. The significance marked on the lines represents the differences between the two groups connected by the lines.

NF-κB was preliminarily excluded. Collectively, our study provides a new lead compound for the development of RIPK1 inhibitors. The inhibitory activity of 4–155 is confined to necroptosis, which is beneficial for the treatment of inflammatory and infectious diseases. Meanwhile, the *in vivo* protective effect of 4–155 on SIRS was stronger than sepsis. Sepsis is a complex injury of multiple organ failure caused by infection and inflammation, which cannot be completely resolved by anti-inflammatory therapy alone [49]. Currently, many studies have shown that anti-inflammatory drugs combined with antibiotics or anticoagulants are promising for treating sepsis [50]. Nevertheless, 4–155 alone showed significant protective effects in the classical sepsis model. RIPK1 inhibitor has been widely studied for drug development in many diseases, such as SIRS, sepsis, neurodegenerative diseases, and ischemic injury. The enhanced efficiency of 4–155 *in vivo* may mainly be attributed to its high activity, as the concentrations of 4–155 against necroptosis were reduced by about 10 times compared to Nec-1 s *in vitro*. Regarding the difference in activity between 4–155 and Nec-1 s, there are two possible reasons. First, the binding sites of 4–155 and Nec-1 s may be different. According to the binding sites, RIPK1 inhibitors are mainly divided into four categories, including type I ATPase inhibitors, type II ATPase inhibitors, type III kinase inhibitors, and others [51]. Nec-1 s with indole hydantoin as its core structure was shown to occupy an allosteric lipophilic pocket on the backside of the ATP-binding site, belonging to the type III kinase inhibitors [52, 53]. Some of type I ATPase inhibitors, type II ATPase inhibitors, and RIPK1 inhibitors with other binding sites may have higher activities than type III kinase inhibitors [54, 55] The core structure of 4–155 is benzoxazepine, and the chemical structure of 4–155 is quite different from that of Nec-1 s. Therefore, we speculated that the binding site of 4–155 might be different with Nec-1 s. Nevertheless, 4–155 still cannot be ruled out as a type III kinase inhibitor. It might act as a type III kinase inhibitor with greater affinity and higher intrinsic activity. Further structural studies are required to reveal the detailed binding information of RIPK1 and 4–155. In addition, the high *in vivo* efficiency of 4–155 indicated that 4–155 also had good pharmacokinetic properties. In future studies, we would investigate the pharmacokinetic properties of 4–155 to provide more evidence for its druggability.

Collectively, our study identified a novel anti-inflammatory lead compound 4–155 that protects mice from SIRS and sepsis by inhibiting the function of RIPK1. Subsequent studies on 4–155 will promote the development of anti-inflammatory drugs.

AUTHOR CONTRIBUTION

All authors contributed to the study conception and design. CLZ and YW conceived and designed this study; QZL, RYL, LLC, and WHX designed experiments and analyzed data; ZYL performed experiments and analyzed data; JL designed and synthesized compound 4–155; QZL and YW wrote and revised the manuscript.

FUNDING

This work was funded by grants from the National Key R&D Program of China (2021YFA1302200), the National Natural Science Foundation of China (82022065, 81772124), Shanghai "Shuguang" Project (21SG38), and the Science and Technology Commission of Shanghai Municipality (21S11900800).

AVAILABILITY OF DATA AND MATERIALS

Data and materials will be made available on request.

DECLARATIONS

Ethics Approval This study was performed in line with the approval granted by the Animal Care Committee of the Second Military Medical University (Shanghai, China).

Competing Interests The authors declare no competing interests.

REFERENCES

1. Mignot-Evers, L., V. Raaijmakers, G. Buunk, S. Brouns, L. Romano, T. van Herpt, *et al*. 2021. Comparison of SIRS criteria and qSOFA score for identifying culture-positive sepsis in the emergency department: A prospective cross-sectional multicentre study. *British Medical Journal Open* 11.
2. Chakraborty, R.K., and B. Burns. 2022 Systemic inflammatory response syndrome. In: StatPearls. Treasure Island (FL).
3. Berkow, E.L., S.R. Lockhart, and L. Ostrosky-Zeichner. Antifungal susceptibility testing: current approaches. Clin Microbiol Rev 2020;33.
4. Ruan, H., D. Ke, and D. Liao. 2022. Prognostic Accuracy of qSOFA and SIRS for Mortality in the emergency department: A meta-analysis and systematic review of prospective studies. *Emergency Medicine International* 2022: 1802707.

5. Rudd, K.E., S.C. Johnson, K.M. Agesa, K.A. Shackelford, D. Tsoi, D.R. Kievlan, *et al*. 2020. Global, regional, and national sepsis incidence and mortality, 1990–2017: Analysis for the Global Burden of Disease Study. *Lancet* 395: 200–211.
6. Fleischmann-Struzek, C., and D. Schwarzkopf. 2022. Reinhart K [Sepsis incidence in Germany and worldwide : Current knowledge and limitations of research using health claims data]. *Medizinische Klinik - Intensivmedizin und Notfallmedizin* 117: 264–268.
7. Septimus, E.J. 2020. Sepsis Perspective 2020. *Journal of Infectious Diseases* 222: S71–S73.
8. Vandewalle, J., and C. Libert. 2020. Glucocorticoids in sepsis: To be or not to be. *Frontiers in Immunology* 11: 1318.
9. Cavaillon, J.M. 2018. Exotoxins and endotoxins: Inducers of inflammatory cytokines. *Toxicon* 149: 45–53.
10. Wang, L., X. Shi, S. Zheng, and S. Xu. 2020. Selenium deficiency exacerbates LPS-induced necroptosis by regulating miR-16-5p targeting PI3K in chicken tracheal tissue. *Metallomics* 12: 562–571.
11. Kaczmarek, A., P. Vandenabeele, and D.V. Krysko. 2013. Necroptosis: The release of damage-associated molecular patterns and its physiological relevance. *Immunity* 38: 209–223.
12. Chen, J., R. Kos, J. Garssen, and F. Redegeld. 2019. Molecular insights into the mechanism of necroptosis: the necrosome as a potential therapeutic target. Cells-Basel. 8.
13. Degterev, A., D. Ofengeim, and J. Yuan. 2019. Targeting RIPK1 for the treatment of human diseases. *Proceedings of the National academy of Sciences of the United States of America* 116: 9714–9722.
14. Newton, K. 2015. RIPK1 and RIPK3: Critical regulators of inflammation and cell death. *Trends in Cell Biology* 25: 347–353.
15. Zarrin, A.A., K. Bao, P. Lupardus, and D. Vucic. 2021. Kinase inhibition in autoimmunity and inflammation. *Nature Reviews. Drug Discovery* 20: 39–63.
16. Duprez, L., N. Takahashi, F. Van Hauwermeiren, B. Vandendriessche, V. Goossens, T. Vanden Berghe, *et al*. 2011. RIP kinase-dependent necrosis drives lethal systemic inflammatory response syndrome. *Immunity* 35: 908–918.
17. Oeckinghaus, A., M.S. Hayden, and S. Ghosh. 2011. Crosstalk in NF-kappaB signaling pathways. *Nature Immunology* 12: 695–708.
18. Mifflin, L., D. Ofengeim, and J.Y. Yuan. 2020. Receptor-interacting protein kinase 1 (RIPK1) as a therapeutic target. *Nature Reviews Drug Discovery* 19: 553–571.
19. Chen, L.Z.X., Y. Ou, M. Liu, D. Yu, Z. Song, L. Niu, L. Zhang, and J. Shi. 2022. Advances in RIPK1 kinase inhibitors. Front Pharmacol. 13.
20. Degterev, A., J.L. Maki, and J. Yuan. 2013. Activity and specificity of necrostatin-1, small-molecule inhibitor of RIP1 kinase. *Cell Death and Differentiation* 20: 366.
21. Zhang, X., H. Zhang, C. Xu, X. Li, M. Li, X. Wu, *et al*. 2019. Ubiquitination of RIPK1 suppresses programmed cell death by regulating RIPK1 kinase activation during embryogenesis. *Nature Communications* 10: 4158.
22. Huang, X., S. Tan, Y. Li, S. Cao, X. Li, H. Pan, *et al*. 2021. Caspase inhibition prolongs inflammation by promoting a signaling complex with activated RIPK1. *Journal of Cell Biology* 220.
23. Xia, C., Z. Yao, L. Xu, W. Zhang, H. Chen, and C. Zhuang. 2021. Structure-based bioisosterism design of thio-benzoxazepinones as novel necroptosis inhibitors. *European Journal of Medicinal Chemistry* 220.
24. Chen, X., C. Zhuang, Y. Ren, H. Zhang, X. Qin, L. Hu, *et al*. 2019. Identification of the Raf kinase inhibitor TAK-632 and its analogues as potent inhibitors of necroptosis by targeting RIPK1 and RIPK3. *British Journal of Pharmacology* 176: 2095–2108.
25. Lomphithak, T., P. Akara-Amornthum, K. Murakami, M. Hashimoto, H. Usubuchi, E. Iwabuchi, *et al*. 2021. Tumor necroptosis is correlated with a favorable immune cell signature and programmed death-ligand 1 expression in cholangiocarcinoma. *Science and Reports* 11: 11743.
26. Xu, J., K.Q. Wang, W.H. Xu, Y.H. Li, Y. Qi, H.Y. Wu, *et al*. 2016. The matrine derivate MASM prolongs survival, attenuates inflammation, and reduces organ injury in murine established lethal sepsis. *Journal of Infectious Diseases* 214: 1762–1772.
27. Zhu, J., M. Xin, C. Xu, Y. He, W. Zhang, Z. Wang, *et al*. 2021. Ligand-based substituent-anchoring design of selective receptor-interacting protein kinase 1 necroptosis inhibitors for ulcerative colitis therapy. *Acta Pharm Sin B* 11: 3193–3205.
28. Zhang, J.X., W.H. Xu, X.H. Xing, L.L. Chen, Q.J. Zhao, and Y. Wang. 2022. ARG1 as a promising biomarker for sepsis diagnosis and prognosis: evidence from WGCNA and PPI network. *Hereditas* 159.
29. Pasparakis, M., and P. Vandenabeele. 2015. Necroptosis and its role in inflammation. *Nature* 517: 311–320.
30. Ofengeim, D., S. Mazzitelli, Y. Ito, J.P. DeWitt, L. Mifflin, C. Zou, *et al*. 2017. RIPK1 mediates a disease-associated microglial response in Alzheimer's disease. *Proceedings of the National Academy of Sciences of United States of America* 114: E8788–E8797.
31. Degterev, A., J. Hitomi, M. Germscheid, I.L. Ch'en, O. Korkina, X. Teng, *et al*. 2008. Identification of RIP1 kinase as a specific cellular target of necrostatins. *Nature Chemical Biology* 4: 313–321.
32. Degterev, A., Z. Huang, M. Boyce, Y. Li, P. Jagtap, N. Mizushima, *et al*. 2005. Chemical inhibitor of nonapoptotic cell death with therapeutic potential for ischemic brain injury. *Nature Chemical Biology* 1: 112–119.
33. Pai, M.Y., B. Lomenick, H. Hwang, R. Schiestl, W. McBride, J.A. Loo, *et al*. 2015. Drug affinity responsive target stability (DARTS) for small-molecule target identification. *Methods in Molecular Biology* 1263: 287–298.
34. Zhang, H., X. Wu, X. Li, M. Li, F. Li, L. Wang, *et al*. 2020. Crucial roles of the RIP homotypic interaction motifs of RIPK3 in RIPK1-dependent cell death and lymphoproliferative disease. *Cell Reports* 31.
35. Mompean, M., W. Li, J. Li, S. Laage, A.B. Siemer, G. Bozkurt, *et al*. 2018. The structure of the necrosome RIPK1-RIPK3 core, a human hetero-amyloid signaling complex. *Cell* 173 (1244–53).
36. Takahashi, N., L. Duprez, S. Grootjans, A. Cauwels, W. Nerinckx, J.B. DuHadaway, *et al*. 2012. Necrostatin-1 analogues: Critical issues on the specificity, activity and *in vivo* use in experimental disease models. *Cell Death & Disease* 3.
37. Qi, W., and J. Yuan. 2022. RIPK1 and RIPK3 form mosaic necrosomes. *Nature Cell Biology* 24: 406–407.
38. Iorga, A., K. Donovan, L. Shojaie, H. Johnson, J. Kwok, J. Suda, *et al*. 2021. Interaction of RIPK1 and A20 modulates MAPK signaling in murine acetaminophen toxicity. *Journal of Biological Chemistry* 296.
39. Gao, Y.L., J.H. Zhai, and Y.F. Chai. 2018. Recent advances in the molecular mechanisms underlying pyroptosis in sepsis. *Mediators of Inflammation* 2018: 5823823.
40. Gaddis, M.L., and Gaddis, G.M. 2021. Detecting sepsis in an emergency department: SIRS vs. qSOFA. *MoMed* 118:253–8.
41. Wang, Y., H. Ma, J. Huang, Z. Yao, J. Yu, W. Zhang, *et al*. 2021. Discovery of bardoxolone derivatives as novel orally active necroptosis inhibitors. *European Journal of Medicinal Chemistry* 212.
42. Wang, X., Y. Chai, Z. Guo, Z. Wang, H. Liao, Z. Wang, *et al*. 2023. A new perspective on the potential application of RIPK1 in the treatment of sepsis. *Immunotherapy*.

43. Xu, G., Y. Li, S. Zhang, H. Peng, Y. Wang, D. Li, *et al*. 2021. SARS-CoV-2 promotes RIPK1 activation to facilitate viral propagation. *Cell Research* 31: 1230–1243.
44. Tao, P., J. Sun, Z. Wu, S. Wang, J. Wang, W. Li, *et al*. 2020. A dominant autoinflammatory disease caused by non-cleavable variants of RIPK1. *Nature* 577: 109–114.
45. Newton, K., V.M. Dixit, and N. Kayagaki. 2021. Dying cells fan the flames of inflammation. *Science* 374: 1076–1080.
46. Jin, L., P. Liu, M. Yin, M. Zhang, Y. Kuang, and W. Zhu. 2020. RIPK1: A rising star in inflammatory and neoplastic skin diseases. *Journal of Dermatological Science* 99: 146–151.
47. Harris, P.A. 2021. Inhibitors of RIP1 kinase: A patent review (2016-present). *Expert Opinion on Therapeutic Patents* 31: 137–151.
48. Christofferson, D.E., Y. Li, J. Hitomi, W. Zhou, C. Upperman, H. Zhu, *et al*. 2012. A novel role for RIP1 kinase in mediating TNFalpha production. *Cell Death & Disease* 3.
49. Evans, T. 2018. Diagnosis and management of sepsis. *Clinical Medicine (London, England)* 18: 146–149.
50. Jarczak, D., S. Kluge, and A. Nierhaus. 2021. *Sepsis-pathophysiology and therapeutic concepts. Front Med (Lausanne)* 8.
51. Chen, L., X. Zhang, Y. Ou, M. Liu, D. Yu, Z. Song, *et al*. 2022. Advances in RIPK1 kinase inhibitors. *Frontiers in Pharmacology* 13.
52. Xie, T., W. Peng, Y. Liu, C. Yan, J. Maki, A. Degterev, *et al*. 2013. Structural basis of RIP1 inhibition by necrostatins. *Structure* 21: 493–499.
53. Najjar, M., C. Suebsuwong, S.S. Ray, R.J. Thapa, J.L. Maki, S. Nogusa, *et al*. 2015. Structure guided design of potent and selective ponatinib-based hybrid inhibitors for RIPK1. *Cell Reports* 10: 1850–1860.
54. Zhou, T., Q. Wang, N. Phan, J. Ren, H. Yang, C.C. Feldman, J.B. Feltenberger, *et al*. 2019. Identification of a novel class of RIP1/RIP3 dual inhibitors that impede cell death and inflammation in mouse abdominal aortic aneurysm models. *Cell Death & Disease* 10(3):226.
55. Xu, L., and C. Zhuang. 2023. Profiling of small-molecule necroptosis inhibitors based on the subpockets of kinase–ligand interactions. *Medicinal Research Reviews* 1–51